Math. Model. Nat. Phenom.
Vol. 8, No. 3, 2013, pp. 182–197
DOI: 10.1051/mmnp/20138311

Finite Element Computation of KPP Front Speeds in 3D Cellular and ABC Flows

L. Shen[1], J. Xin[2*], A. Zhou[3]

[1] School of Mathematics, Capital Normal University, Beijing 100048, China

[2] Department of Mathematics, University of California at Irvine, Irvine, CA 92697, USA

[3] LSEC,Institute of Computational Mathematics and Scientific/Engineering Computing, Academy of Mathematics and Systems Science, Chinese Academy of Sciences, Beijing 100190, China

Abstract. We carried out a computational study of propagation speeds of reaction-diffusion-advection fronts in three dimensional (3D) cellular and Arnold-Beltrami-Childress (ABC) flows with Kolmogorov-Petrovsky-Piskunov(KPP) nonlinearity. The variational principle of front speeds reduces the problem to a principal eigenvalue calculation. An adaptive streamline diffusion finite element method is used in the advection dominated regime. Numerical results showed that the front speeds are enhanced in cellular flows according to sublinear power law $O(\delta^p)$, $p \approx 0.13$, δ the flow intensity. In ABC flows however, the enhancement is $O(\delta)$ which can be attributed to the presence of principal vortex tubes in the streamlines. Poincaré sections are used to visualize and quantify the chaotic fractions of ABC flows in the phase space. The effect of chaotic streamlines of ABC flows on front speeds is studied by varying the three parameters (a, b, c) of the ABC flows. Speed enhancement along x direction is reduced as b (the parameter controling the flow variation along x) increases at fixed $(a, c) > 0$, more rapidly as the corresponding ABC streamlines become more chaotic.

Keywords and phrases: KPP fronts, 3D Cellular and ABC Flows, eigenvalue problems, adaptive streamline diffusion finite element method.

Mathematics Subject Classification: 65C30, 65C05, 65N30, 65N25

1. Introduction

Front propagation in fluid flows is a robust nonlinear phenomenon in premixed turbulent combustion and reactive transport among other scientific areas [10, 14, 26, 31, 33, 39, 42, 43, 45]. A fundamental problem is to analyze and compute large scale front speeds in complex flows. Much progress has been made in recent years for the Kolmogorov-Petrovsky-Piskunov (KPP) reactive fronts in the large amplitude regime of steady periodic incompressible flows [1, 3, 30, 35, 46]. An extensively studied example is the two dimensional cellular flow consisting of periodic array of vortices. The KPP equation is:

$$u_t = \kappa \Delta_{\mathbf{z}} u + \mathbf{B}(\mathbf{z}) \cdot \nabla_{\mathbf{z}} u + \frac{1}{\tau_r} f(u), \quad \mathbf{z} \in \mathbb{R}^n, \quad t > 0, \tag{1.1}$$

*Corresponding author. E-mail: jxin@math.uci.edu

© EDP Sciences, 2013

Article published by EDP Sciences and available at http://www.mmnp-journal.org or http://dx.doi.org/10.1051/mmnp/20138311
https://doi.org/10.1051/mmnp/20138311 Published online by Cambridge University Press

where κ and τ_r are two positive constants, $\mathbf{B}$ is a given steady incompressible 2π-periodic velocity field; $f(u) = u(1-u)$, the so called KPP nonlinearity.

In this paper, we shall carry out a numerical study of KPP front speeds of equation (1.1) in a three dimensional (3D) infinite cylinder $\mathbf{z} = (x, y, z) \in \mathbb{R}^1 \times [0, L_y] \times [0, L_z]$, where L_y and L_z are positive constants. The boundary condition is zero Neumann. If the initial data for u is nonnegative and front-like (approaching zero and one rapidly enough as $x \to \pm\infty$), large time behavior of u is a propagating front along x. We will denote the KPP front speed as μ which admits a variational characterization in terms of principal eigenvalue of an associated linear operator [7,43]. More precisely, let $\Omega = [0, 2\pi]\times[0, L_y]\times[0, L_z]$, and for each fixed λ, we consider the principal eigenvalue problem of (H, ϕ) with zero Neumann boundary condition at $y = 0, L_y$; $z = 0, L_z$; 2π-periodic in x:

$$\begin{aligned} &\kappa\Delta\phi + (2\kappa\lambda\boldsymbol{e} + \mathbf{B}) \cdot \nabla\phi + [\kappa\lambda^2 + \lambda\boldsymbol{e} \cdot \mathbf{B} + \tau^{-1} f'(0)]\phi = H(\lambda)\phi, \qquad \text{in } \Omega, \\ &\phi|_{x=0} = \phi|_{x=L_x}, \quad \frac{\partial\phi}{\partial\nu}|_{y=0,L_y} = 0, \quad \frac{\partial\phi}{\partial\nu}|_{z=0,L_z} = 0, \end{aligned} \tag{1.2}$$

where ν is the outer normal vector, $\boldsymbol{e} = (1, 0, 0)$, B is a 2π-periodic incompressible flow field, either a 3-D cellular flow or an Arnold-Beltrami-Childress (ABC) flow. The 3-D cellular flow is:

$$\mathbf{B}(x, y, z) = (\Phi_x(x, y)W'(z), \Phi_y(x, y)W'(z), k\Phi(x, y)W(z)), \tag{1.3}$$

with $-\Delta\Phi = k\Phi$. In our computation, we shall fix $k = 2$, or

$$\mathbf{B}(x, y, z) = (-\sin x \cos y \cos z, -\cos x \sin y \cos z, 2\cos x \cos y \sin z).$$

The ABC flow field is:

$$\mathbf{B}(x, y, z) = (a\sin(z) + c\cos(y), b\sin(x) + a\cos(z), c\sin(y) + b\cos(x)), \tag{1.4}$$

parametrized by 3 constants (a, b, c), whose streamlines are known to be chaotic in certain regimes [17]. ABC flows have been studied as prototype flows for flow enhanced diffusion and dynamo problems [9,12,18,21,22,32], however, little appears to be known of their properties in front propagation problems.

The KPP front speed along $\boldsymbol{e}$ is given by:

$$\mu = \inf_{\lambda>0} \frac{H(\lambda)}{\lambda}, \tag{1.5}$$

where $H(\lambda)$ is the largest eigenvalue of (1.2). The variational formula (1.5) makes possible accurate and efficient computation of KPP front speeds without direct simulation of the time-dependent reaction-diffusion-advection equation (1.1). For random flows, computation based on variants of (1.5) are performed in [29, 36]. In [36], the present authors initiated a numerical study for KPP front speeds in random shear flows using two-scale finite element methods. They also computed KPP front speeds in 2-D periodic cellular flows and cat's eye flows based on an adaptive streamline diffusion finite element method [37]. If the flow field is scaled as $\mathbf{B}(x, y) \to \delta \cdot \mathbf{B}(x, y)$ for a positive constant δ, we are interested in the dependence of front speed on δ when δ is large. At large δ, the eigenfunction ϕ develops internal layers, for which an adaptive finite element method is appropriate. We shall also study the effect of chaos in ABC flows and the (a, b, c) parameters on the propagation speed μ. The amount of chaos in the phase space of a 3D flow is measured by volume fractions occupied by dense points on the Poincaré sections.

The rest of the paper is organized as follows. In section 2, we give a brief overview of the asymptotic theory of KPP front speeds in the large δ limit and ABC flows. In section 3, we present adaptive and streamline diffusion finite element methods for computation of eigenvalue problem (1.2). In section 4, we present numerical results on KPP front speeds μ in 3D cellular flows and ABC flows. We observed that the sublinear growth of front speeds in cellular flows in the large advection regime (large δ) is a power law of $O(\delta^p)$, $p \approx 0.13$, in constrast $p = 0.25$ in 2D [3,30]. In ABC flows, the speed growth is linear or $O(\delta)$ at

https://doi.org/10.1051/mmnp/20138311 Published online by Cambridge University Press

large δ. The speed is monotone increasing in c at fixed (a, b), and monotone decreasing in b at fixed (a, c). The qualitative behavior may be attributed to c controling the y dependence of the flow field which is in a perpendicular direction to front motion in x, while b controls the x dependence of the flow. The former is analogous to shear flows which enhance front speeds and the latter mimics compresssible flows which decrease front speeds. Similar to the former case, the front speed μ is monotone increasing in a at fixed (b, c). Geometrically, the presence of vortex tubes (principal vortices [17]) in the ABC flows is associated with the linear growth. The related maximally enhanced diffusion was confirmed numerically before [9]. If none of the (a, b, c) parameters is equal to zero, the ABC flow is non-integrable and chaotic regions may exist around the vortex tubes. We found that as the volume fractions of the chaotic regions peak with increasing and uniformly sampled values of $b = \sqrt{1/3}\, i$ $(i = 1, 2, 3, 4)$ at fixed $(a, c) = (1, \sqrt{1/3})$, the reduction of front speed tends to intensify in a nonlinear manner. In contrast, as the volume fractions of the chaotic regions peak with increasing and uniformly sampled values of $c = \sqrt{1/3}\, i$ $(i = 1, 2, 3, 4)$ at fixed $(a, b) = (1, \sqrt{2/3})$, the speed growth rate (μ/δ) is linear in c, showing minimal influence from chaotic streamlines in ABC flows. The result is similar as a varies at fixed (b, c). In section 5, we conclude with remarks on future work of computing KPP front speeds in three dimensional flows. Our acknowledgements are in section 6.

2. Overview of KPP front speeds and ABC flows

Qualitative properties of KPP front speeds in two and higher dimensional periodic steady flows have been actively studied in recent years in the large flow amplitude regime. For 2D cellular flows at large δ, $\mu(\delta) \sim O(\delta^{1/4})$ in any direction of propagation [3, 30]. If the Hamiltonian of the 2D cellular flow is perturbed periodically into that of the cat's eye flow [12, 20], $\mu(\delta) = O(1)$ in the direction $(-1, 1)/\sqrt{2}$ and $O(\delta)$ in any other direction [44]. In three and higher dimensions, asymptotic results are less precise. There are Eulerian type criteria on bounded or unbounded behavior of μ as $\delta \to +\infty$ in terms of the existence of H^1 solution (first integral) of the equation $\mathbf{B} \cdot (\nabla w - \boldsymbol{e}) = 0$ on the torus [8, 35]. The Lagrangian criterion on the linear growth rate of μ in δ is given in terms of the large time behavior of the orbit of the flow field $\mathbf{B}$ [44]. In other words, there exists an orbit or a smooth solution of $\xi' = \mathbf{B}(\xi(t))$ such that

$$\lim_{t\to+\infty} \boldsymbol{e} \cdot \xi(t)/t = \lim_{\delta\to+\infty} \mu(\delta)/\delta. \tag{2.1}$$

For 3D cellular flows (1.3) as illustrated in Figure 1, it is shown in [35] that

$$\mu(\delta) \to +\infty, \ \text{ as } \ \delta \to +\infty. \tag{2.2}$$

By the Lagrangian criterion [44],

$$\mu(\delta)/\delta \to 0, \ \text{ as } \ \delta \to +\infty. \tag{2.3}$$

The variational formula of the linear growth rate in R^n is [46] (take $\tau_r = 1$ for simplicity):

$$\lim_{\delta\to+\infty} \frac{\mu(\delta)}{\delta} = \sup_{w\in I, \|\nabla w\|_2^2 \le f'(0)\|w\|_2^2} \frac{\int_{T^n} (\mathbf{B}\cdot\boldsymbol{e})\, w^2}{\|w\|_2^2}, \tag{2.4}$$

where $I = \{w \in H^1(T^n) : \mathbf{B} \cdot \nabla w = 0\}$, the set of first integrals of vector field $\mathbf{B}$ on the n-dimensional torus T^n $(n \ge 3)$.

No analytical results appear to be known about μ in ABC flows, though a lot is known about streamlines of the ABC flows [17]. By symmetry, it suffices to consider $(a, b, c) \ge 0$. In case of $1 = a \ge b \ge c \ge 0$, stagnation points exist if $b^2 + c^2 \ge 1$. Other stagnation conditions follow by permuating a, b, c. There are six so called principal vortex tube regions in ABC flows, two along each axis where Lagrangian particles move predominantly in one direction. Outside of these vortical tubes, chaotic streamlines exist due to unstable periodic orbits, stagnation points, heteroclinic orbits etc. Poincaré sections can be used for flow visualization and as a quantitative measure as we shall present later. It would be interesting to show that

https://doi.org/10.1051/mmnp/20138311 Published online by Cambridge University Press

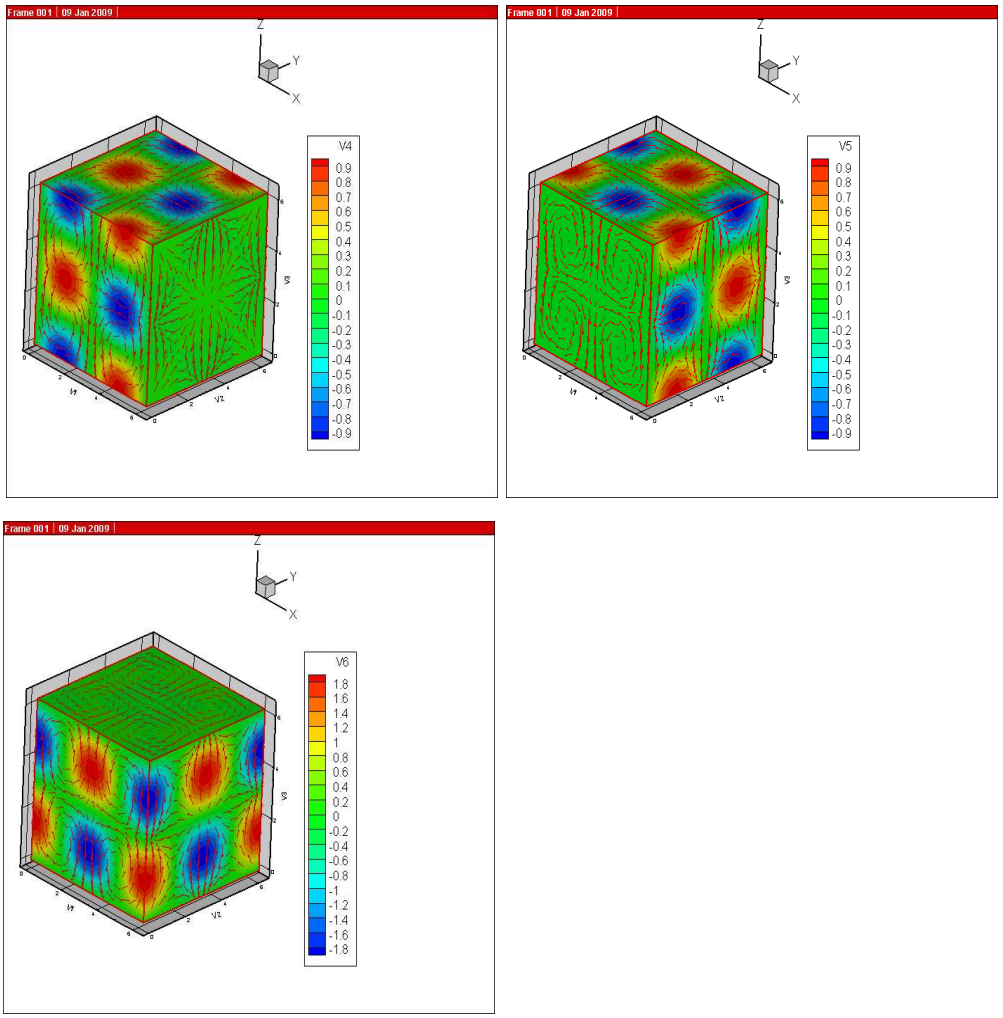


FIGURE 1. The 3-D cellular flow and the values of its x (upper left), y (upper right) and z (lower left) components with vector field.

the right hand side of (2.4) is positive for $\mathbf{B}$ equal to the ABC flow. We shall demonstrate this property numerically, and study the more subtle effects of chaotic regions on the behavior of μ.

With scaling $\mathbf{B} \to \delta\mathbf{B}$, we compute the front speeds $\mu(\delta) = \inf_{\lambda>0} \dfrac{H(\lambda,\delta)}{\lambda}$ where with fixed δ the function $\dfrac{H(\lambda,\delta)}{\lambda}$ is a convex function of λ and the minimum point is unique. The ABC flows are illustrated in Figure 2.

3. Numerical Problem and Methods

Since ABC flow is 2π-periodic, we confine the domain to the cubic $[0,2\pi]\times[0,2\pi]\times[0,2\pi]$. That is , choose $L_x = L_y = L_z = 2\pi$. Equation (1.2) becomes the following eigenvalue problem:

$$\kappa\Delta\phi + (2\kappa\lambda\boldsymbol{e} + \mathbf{B})\cdot\nabla\phi + [\kappa\lambda^2 + \lambda\boldsymbol{e}\cdot\mathbf{B} + \tau^{-1}f'(0)]\phi = H(\lambda)\phi, \quad \text{in } \Omega,$$

$$\phi|_{x=0} = \phi|_{x=2\pi}, \quad \frac{\partial\phi}{\partial\nu}|_{y=0,2\pi} = 0, \quad \frac{\partial\phi}{\partial\nu}|_{z=0,2\pi} = 0, \tag{3.1}$$

https://doi.org/10.1051/mmnp/20138311 Published online by Cambridge University Press

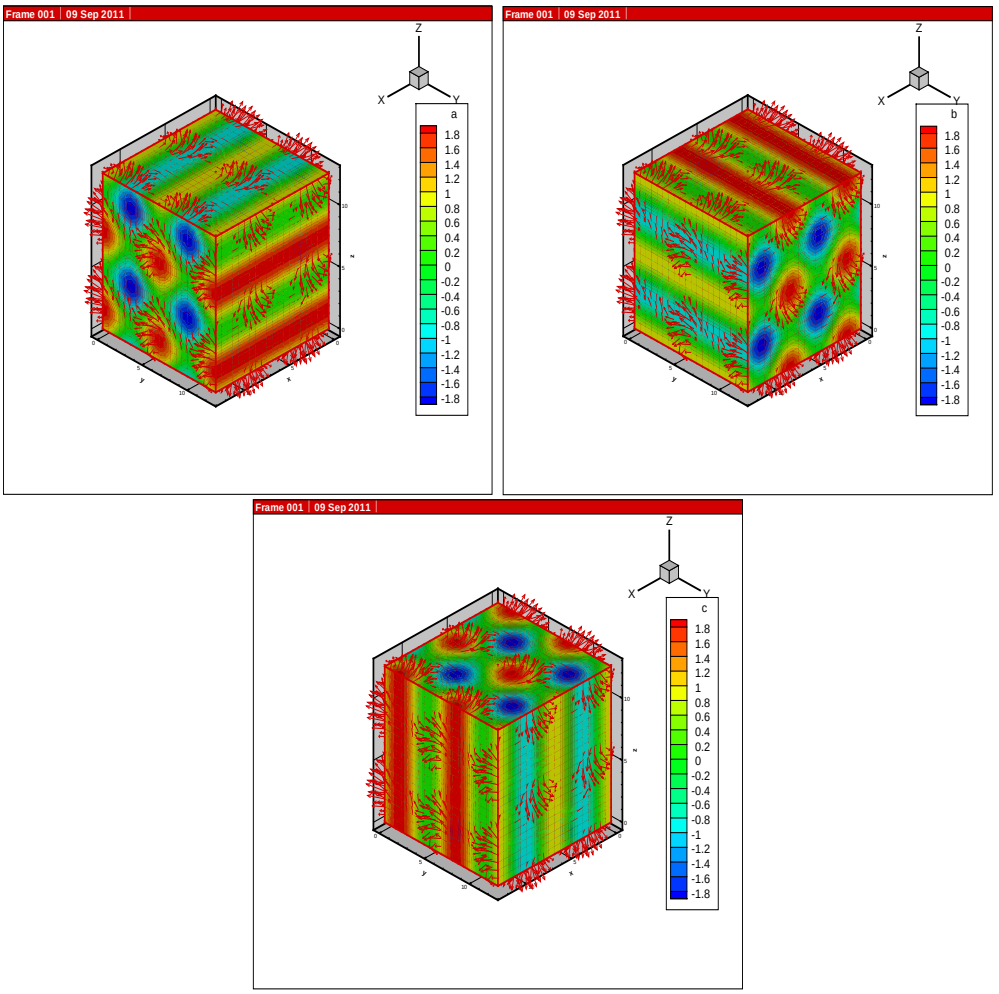


FIGURE 2. The x (up-left), y (up-right), z (bottom) component values of the ABC flow and the vector field in the domain $[0, 4\pi] \times [0, 4\pi] \times [0, 4\pi]$.

where $\kappa = 1.0$ and $\tau = 2.0$.

To simplify presentation, we denote $\tilde{\mathbf{B}} = (\tilde{B}_x, \tilde{B}_y, \tilde{B}_z) = 2\kappa\lambda\mathbf{e} + \delta\mathbf{B}(x, y, z)$, and $\tilde{C} = \kappa\lambda^2 + \lambda\delta\mathbf{e} \cdot \mathbf{B}(x, y, z) + \tau^{-1}f'(0)$. The first equation of (1.2) has the form

$$\kappa\Delta\phi + \tilde{\mathbf{B}} \cdot \nabla\phi + \tilde{C}\phi = H(\lambda)\phi \ . \tag{3.2}$$

According to the dominance of convection, i.e., the various values of δ, we choose the standard finite element method, the streamline diffusion method and the adaptive streamline diffusion method to solve this problem and obtain the eigenvalue and the corresponding eigenfunction. For a fixed δ, when the eigenvalues $H(\lambda)$ are obtained at different values of λ, we find the approximation of the unique minimal value of $\dfrac{H(\lambda)}{\lambda}$ based on its strict convexity.

The streamline diffusion method is widely used in convection dominated problems to stabilize the discretization methods. The method was originally investigated for solving the boundary value problems by Hughes and Brooks [23] and then analyzed by Nävert [28] and Johnson et al [24] (see also [25,34] and references cited therein). As an efficient computational method, we understand that the adaptive finite

https://doi.org/10.1051/mmnp/20138311 Published online by Cambridge University Press

element method has been extensively studied. We refer to Babuška and Vogelius [5] for one dimensional linear symmetric elliptic problems and [16, 27, 40] for higher dimensional boundary value problems and eigenvalue problems. The combination of those two methods is the adaptive streamline diffusion method which was applied to stationary convection-diffusion (boundary value) problems by Johnson and his co-workers [19]. It was also applied by the authors to a two-dimensional convection dominated eigenvalue problem [37] in which it was compared with the standard finite element method and upwind finite difference method to show its high efficiency. However, to our best knowledge, there is no work applying the streamline diffusion method to solve an eigenvalue problem in three dimensions. Computation is challenging due to convection dominance, nonlinear nature and high dimension of the problem. It takes more sophisticated construction of mesh refinements and streamline diffusion function, as well as parallel computing.

3.1. Standard finite element method

We define a bilinear form

$$a(w,v) = -(\kappa\nabla w, \nabla v) + (\tilde{\mathbf{B}}\cdot\nabla w, v) + (\tilde{C}w, v) + \int_{\Omega|_{x=0}\cup\Omega|_{x=2\pi}} \kappa v\nabla w\cdot\mathbf{n}\, ds,\ \forall w, v\in H^1(\Omega), \tag{3.3}$$

and the function space

$$V = \{v\in H^1(\Omega) : v|_{x=0} = v|_{x=2\pi}\},$$

where $(\cdot,\cdot)$ denotes the inner product in $L^2(\Omega)$, $\mathbf{n}$ is the exterior normal at the boundary surfaces $\Omega|_{x=0}$ and $\Omega|_{x=2\pi}$. Then the variational form for equation (1.2) can be written as follows: Find $(H,\phi)\in\mathbb{R}\times V$ such that

$$a(\phi, v) = H(\phi, v), \quad \forall v\in V. \tag{3.4}$$

Let T_h be a shape regular conforming tetrahedral finite element mesh over Ω with size h [2, 11, 38]. Denote the linear finite element space

$$S_h = \{p\in H^1(\Omega) : p|_e \text{ is piecewise linear }, \forall e\in T_h\}$$

and let

$$V_h = S^h\cap V.$$

Then the standard finite element discretization for (3.4) is: Find $(H_h,\phi_h)\in\mathbb{R}\times V_h$ such that

$$a(\phi_h, v) = H_h(\phi_h, v), \quad \forall v\in V_h. \tag{3.5}$$

After discretization, we can get a linear system which is a generalized eigenvalue problem

$$Mu = H_hNu,$$

where M and N are matrices with the same row and column numbers as the number of unknowns. The value H_h is the eigenvalue and the vector u the corresponding eigenvector. We use the inverse power method to solve this eigenpair in our computation since only the smallest eigenvalue is required.

If the coefficients of (1.2) are of the same scale, the convergence and error estimates of approximations of (3.5) are well established [4].

3.2. Streamline diffusion finite element method(SD-FEM)

Similar to the streamline diffusion finite element method for boundary value problems [25, 34], we define

$$a_h(\phi, v) = a(\phi, v) + \sum_{e\in T_h} c_e(\kappa\Delta\phi + \tilde{\mathbf{B}}\cdot\nabla\phi + \tilde{C}\phi,\ \tilde{\mathbf{B}}\cdot\nabla v)_e, \quad \forall\phi,\ v\in V_h \tag{3.6}$$

https://doi.org/10.1051/mmnp/20138311 Published online by Cambridge University Press

and

$$b_h(\phi, v) = (\phi, v) + \sum_{e \in T_h} c_e(\phi,\ \tilde{\mathbf{B}} \cdot \nabla v)_e, \quad \forall \phi,\ v \in V_h, \tag{3.7}$$

where $(\cdot, \cdot)_e$ denotes the inner product in $L^2(e)$. In our computation, we choose c_e as follows [15]

$$c_e = \mathrm{O}(H_e), \quad H_e = \frac{1}{\frac{4}{h_e^2} + \frac{2\tilde{\mathbf{B}}}{h_e} + \tilde{C}}.$$

Our streamline diffusion finite element discretization for solving (3.4) is: Find $(H_h^{sd}, \phi_h^{sd}) \in R^1 \times V_h$ such that

$$a_h(\phi_h^{sd},\ v) = H_h^{sd} b_h(\phi_h^{sd},\ v), \quad \forall v \in V_h. \tag{3.8}$$

If the coefficients are of the same scale, the error estimates of the above equation are well studied (see, e.g., [25, 34] and the abstract spectral approximation results in [4]). In this paper, we consider not only the problem with coefficients of the same scale, but also with the convection term being dominant. To our best knowledge, except for the two-dimensional convection dominant problem studied by the authors [37], there is no work applying the streamline diffusion method to solve an eigenvalue problem in such a regime.

3.3. Adaptive streamline diffusion finite element method

To improve the computational efficiency, we combine the streamline diffusion finite element method with the adaptive method. Let T_h be a shape regular conforming tetrahedral finite element mesh and ∂T_h the set of all interior faces (of tetrahedrons) in T_h. The refinement strategy is as follows [27, 40]:

– *Error estimation*
  Compute some local error estimator $\eta_e = \eta_e(\phi_h)$ for all $e \in T_h$.
– *Mark and locally refine*
  Refine those elements $\{e\}$ that satisfy

$$\eta_e(\phi_h) > r \max_{e \in T^h} \eta_e(\phi_h), \tag{3.9}$$

  where $r \in (0,\ 1)$ is a given refinement parameter.

In our local refining, we use the tetrahedron bisection approach [2, 27] to refine the meshes. First, we bisect all the marked tetrahedrons. This may generate hanging nodes. Second, we bisect those tetrahedrons with hanging nodes until all of the hanging nodes are removed and the conforming mesh is obtained.

To describe the adaptive finite element algorithm for (3.8), we shall replace the subscript h by an iteration counter k of the adaptive algorithm afterwards for convenience. Given an initial tetrahedron T_0 with size h_0, we generate a sequence of nested conforming tetrahedrons T_k using the following loop:

$$\text{Solve} \ \rightarrow \ \text{Estimate} \ \rightarrow \ \text{Mark} \ \rightarrow \ \text{Refine}.$$

More precisely, we have an adaptive finite element algorithm for (3.8) as follows:

Algorithm 3.1. *Adaptive finite element algorithm*

1. *Pick an initial mesh T_0 and let $k = 0$.*
2. *Solve (3.8) on T_k and get the finite element eigenpair (H_k^{sd}, ϕ_k^{sd}).*
3. *Compute local error indictors $\eta_e(\phi_k^{sd})\ \ \forall\ e \in T_k$.*
4. *Refine such elements $\{e\}$ in T_k that satisfy*

$$\eta_e(\phi_k^{sd}) > r \max_{e \in T_k} \eta_e(\phi_k^{sd}) \tag{3.10}$$

to get a new conforming mesh T_{k+1}, where $r \in (0,\ 1)$ is a given refinement parameter.

https://doi.org/10.1051/mmnp/20138311 Published online by Cambridge University Press

5. Let $k = k + 1$ and go to 2.

Following [41], we design our local error indictors on each element $e \in T_h$ as

$$\eta_e(\phi_h) = \left(A^{-1} h_e^2 \|R_e(\phi_h)\|_{0,e}^2 + \frac{1}{2} A^{\frac{1}{2}} h_e \|R_l(\phi_h)\|_{0,l}^2 \right)^{\frac{1}{2}} \tag{3.11}$$

and the global a posteriori error estimations as

$$\begin{aligned} \eta(\phi_h) &= \left(\sum_{e \in T_h} \eta_e(\phi_h)^2 \right)^{\frac{1}{2}} \\ &= \left(\sum_{e \in T_h} A^{-1} h_e^2 \|R_e(\phi_h)\|_{0,e}^2 + \sum_{l \in \partial T_h} A^{\frac{1}{2}} h_e \|R_l(\phi_h)\|_{0,l}^2 \right)^{\frac{1}{2}}, \end{aligned} \tag{3.12}$$

where

$$R_e(\phi_h) = H\phi_h - \kappa \Delta \phi_h - \tilde{\mathbf{B}} \nabla \phi_h - \tilde{C} \phi_h$$

and

$$R_l(\phi_h) = \kappa [\frac{\partial \phi_h}{\partial \mathbf{n}}]_l,$$

with l labeling a face of element e and $[\cdot]_l$ denoting the jump across l.

4. Numerical Results

In this section, we present numerical results of equation (3.1) solved by the standard finite element method, the uniform streamline diffusion finite element method and the adaptive streamline diffusion finite element method as we mentioned before. Different methods were chosen for different ranges of δ to balance computational costs and accuracy. For small δ, we use standard finite element method. As the value of δ grows and the standard finite element method becomes unstable, we switch to the uniform streamline diffusion finite element method. When the value of δ gets even larger and it is too costly to get convergent results by the uniform streamline diffusion finite element method, we turn to the adaptive streamline diffusion finite element method. For flows with different parameters, the methods for the same δ value may be different. We shall focus on the variation of front speeds in terms of the parameters a, b, c of the ABC flows.

The ABC flows have both ordered and chaotic streamlines [17]. In Figure 3, we show the eight equidistant Poincaré sections of the chaotic streamlines parallel to the (x, y)-plane at $z = 0$, $\frac{1}{4}\pi$, $\frac{2}{4}\pi$, $\cdots$, $\frac{7}{4}\pi$ for various values of c and $a = 1$, $b = \sqrt{2/3}$. As the value of c decreases from $4\sqrt{2/3}$ to 0, the chaotic region reaches the maximum at $c = 3\sqrt{1/3}$. In Figure 4, the upper left plot shows that the front speed μ increases linearly in δ for different c values. The upper-right plot is a log plot that shows the growth exponent to be one for ABC flows and approximately 0.13 for the 3D cellular flows. The lower-left plot shows the speed growth rates (μ/δ at the largest δ computed) vs. different values of c. The lower-right plot shows the volume fractions of the chaotic streamlines as c varies. The growth rate appears linear in c and is independent of the presence of the chaotic streamlines. The ordered part of the ABC streamlines plays the dominant role.

Figure 5 shows Poincaré sections with $a = 1$, $c = \sqrt{1/3}$ and b varying from $4\sqrt{2/3}$ to 0. The left plot of Figure 6 is on front speed vs. δ, with the right plot on the volume fraction of chaotic streamlines. We see that speed enhancement is reduced more when chaos is getting stronger, alternatively the μ curves spread more between them even as b is uniformly sampled at $b = \sqrt{1/3}, 2\sqrt{1/3}, 3\sqrt{1/3}, 4\sqrt{1/3}$. The chaotic part of streamlines has a nonlinear effect on the front speeds.

Figure 7 shows the Poincaré sections at different values of a.

https://doi.org/10.1051/mmnp/20138311 Published online by Cambridge University Press

In Figure 8, at $b = \sqrt{2/3}$, $c = \sqrt{1/3}$, the front speed is linearly increasing in δ and the speed growth rate is linear in a, similar to Figure 4. Again the ordered part of streamlines dominates.

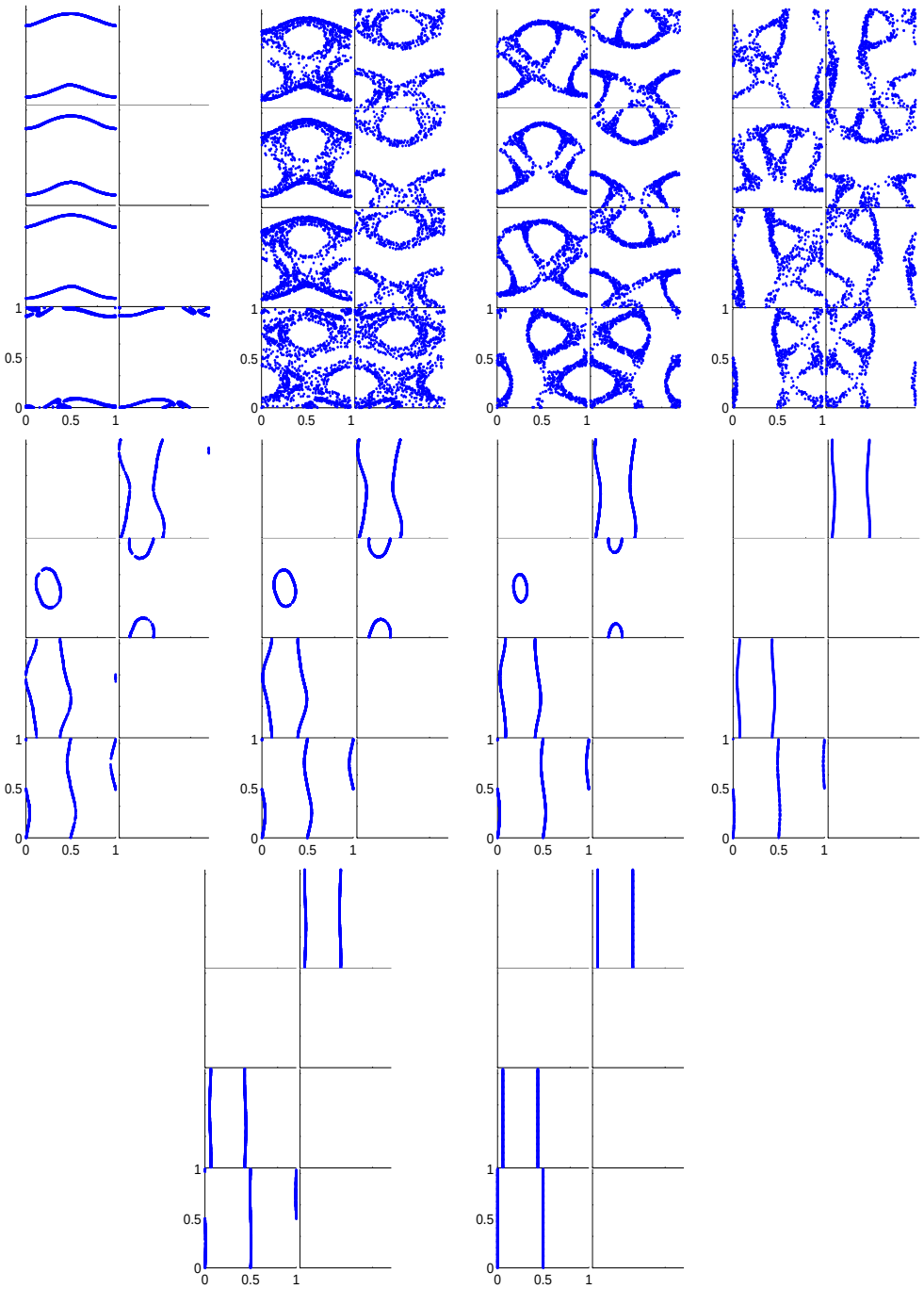


FIGURE 3. The Poincaré sections of the ABC flow. From left to right: $c = 4\sqrt{\frac{1}{3}}$, $3\sqrt{\frac{1}{3}}$, $2\sqrt{\frac{1}{3}}$, $\sqrt{\frac{1}{3}}$, $\frac{7}{8}\sqrt{\frac{1}{3}}$, $\frac{6}{8}\sqrt{\frac{1}{3}}$, $\frac{4}{8}\sqrt{\frac{1}{3}}$, $\frac{2}{8}\sqrt{\frac{1}{3}}$, $\frac{1}{8}\sqrt{\frac{1}{3}}$, 0.

https://doi.org/10.1051/mmnp/20138311 Published online by Cambridge University Press

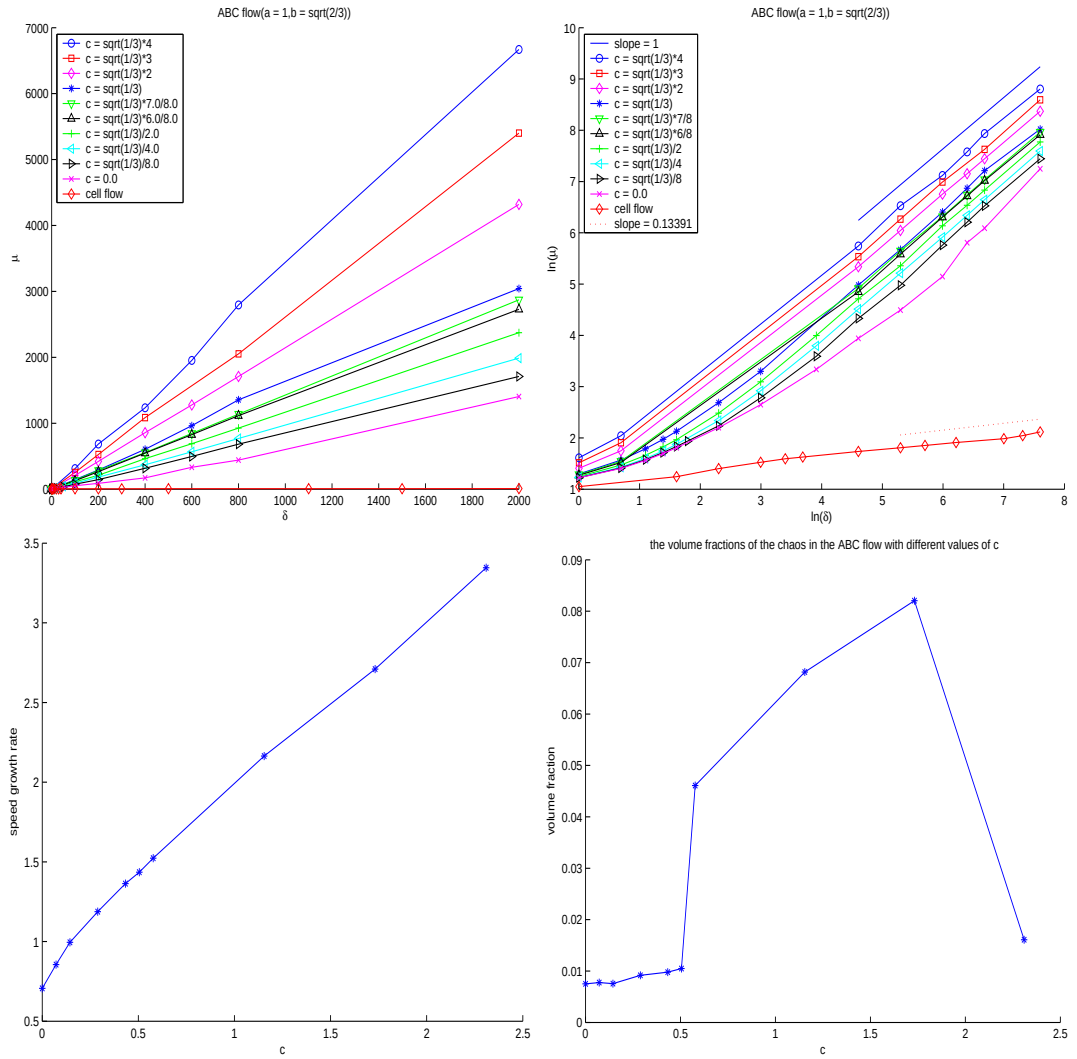


FIGURE 4. The upper-left plot shows the speed growth vs. δ for ABC flows at values of c in Figure 3 and $(a, b) = (1, \sqrt{2/3})$, also 3D cellular flows. The upper-right plot is a log plot on growth exponents. The lower-left plot is on the speed growth rate vs. c values in Figure 3. The lower-right plot is on the volume fraction of the chaotic ABC streamlines with c varying and $(a, b) = (1, \sqrt{2/3})$.

https://doi.org/10.1051/mmnp/20138311 Published online by Cambridge University Press

5. Concluding Remarks

KPP front speeds in 3D cellular flows and ABC flows are computed by a couple of finite element methods especially the adaptive streamline diffusion finite element methods in the advection dominated regime. Numerical results showed the sublinear power law growth of front speeds in cellular flows and linear growth in the ABC flows. The chaotic streamlines in ABC flows play a subtle role in speed enhancement, more pronounced in reducing enhancement as parameter b controling the flow variation in the propagation direction is varied. The instabilities of ABC flows [21] suggest a line of future work on KPP front speeds in time dependent ABC flows.

Acknowledgements. LS was partially supported by National Science Foundation of China under grants 10801101, 10871198 and 11171232. JX was partially supported by NSF under grants DMS-0911277 and DMS-1211179. AZ was partially supported by the Funds for Creative Research Groups of China under grant 11021101, the National Basic Research Program of China under grant 2011CB309703, and the National Center for Mathematics and Interdisciplinary Sciences, Chinese Academy of Sciences. LS would like to thank Dr. Baolin Tian in Beijing Institute of Applied Physics and Computational Mathematics for the valuable discussion and his help in flow fields plotting.

References

[1] M. Abel, M. Cencini, D. Vergni, A. Vulpiani. *Front speed enhancement in cellular flows*. Chaos, 12 (2002), pp. 481–488.
[2] D.N. Arnold, A. Mukherjee, L. Pouly. *Locally adapted tetrahedral meshes using bisection*. SIAM J. Sci. Comput., 22 (2000), pp. 431–448.
[3] B. Audoly, H. Berestycki, Y. Pomeau. *Réaction diffusion en écoulement stationnaire rapide*. C. R. Acad. Sci. Paris 328, Série IIb, 2000, pp. 255–262.
[4] I. Babuška, J.E. Osborn. *Eigenvalue problems*. in: Handbook of Numerical Analysis. Volume II, North-Holland, 1991, pp. 641–787.
[5] I. Babuška, M. Vogelius. *Feedback and adaptive finite element solution of one-dimensional boundary value problems*. Numer. Math., 44 (1984), pp. 75–102.
[6] C. Beattie. *Galerkin eigenvector approximations*. Math. Comput., 69 (2000), pp. 1400–1434.
[7] H. Berestycki, F. Hamel. *Front propagation in periodic excitable media*. Comm. Pure Appl. Math., 55 (2002), pp. 949–1032.
[8] H. Berestycki, F. Hamel, N. Nadirashvili. *Elliptic eigenvalue problems with large drift and applications to nonlinear propagation phenomena*. Comm. Math. Physics, 253 (2005), pp 451–480.
[9] L. Biferale, A. Crisanti, M. Vergassola, A. Vulpiani. *Eddy diffusivities in scalar transport*. Phys. Fluids, 7 (1995), pp. 2725–2734.
[10] A. Bourlioux, B. Khouider. *Rigorous asymptotic perspective on the large scale simulations of turbulent premixed flames*. Multiscale Model. Simul., 6 (2007), pp. 287–307.
[11] J. Brandts, M. Krizek. *Gradient superconvergence on uniform simplicial partitions of polytopes*. IMA J. Numer. Anal., 33 (2003), pp. 1–17.
[12] S. Childress, A.M. Soward. *Scalar transport and alpha-effect for a family of cat's eye flows*. J. Fluid Mech, 205 (1989), pp. 99–133.
[13] P. Clavin, F. Williams. *Theory of premixed-flame propagation in large-scale turbulence*. J. Fluid Mech., 90 (1979), pp. 598–604.
[14] P. Constantin, A. Kiselev, A. Oberman, L. Ryzhik. *Bulk burning rate in passive-reactive diffusion*. Arch. Rat. Mech. Anal., 154 (2000), pp. 53–91.
[15] R Codina. *Comparison of some finite element methods for solving the diffusion-convection-reaction equation*. Comput. Methods Appl. Mech. Engrg. 156 (1998), pp. 185–210.
[16] X. Dai, J. Xu, A. Zhou. *Convergence and optimal complexity of adaptive finite element eigenvalue computations*. Numer. Math., 110 (2008), pp. 313–355.
[17] T. Dombre, U. Frisch, J.M. Greene, M.Hènon, A. Mehr, A.M. Soward. *Chaotic streamlines in the ABC flows,* J. Fluid Mech., 67 (1986), pp. 353–391.
[18] E. Dormy, A. Soward, eds, "Mathematical Aspects of Natural Dynamics", the Fluid Mech. of Astrophysics and Geophysics, Vol. 13, Grenoble Science and CRC Press, 2007.
[19] K. Eriksson, C. Johnson. *Adaptive streamline diffusion finite element methods for stationary convection-diffusion problems*. Math. Comput., 60 (1993), pp. 167–188.
[20] A. Fannjiang, G. Papanicolaou. *Convection enhanced diffusion for periodic flows*. SIAM J. Appl. Math., 54 (1992), pp. 333–408.
[21] S. Friedlander, A. Gilbert, M. Vishik. *Hydrodynamic instability for certain ABC flows*. Geophys. Astrophys. Fluid Dynamics, 73 (1993), pp. 97–107.

https://doi.org/10.1051/mmnp/20138311 Published online by Cambridge University Press

[22] S. Friedlander, M. Vishik. *Dynamo theory, vorticity generation, exponential stretching*. Chaos, 1(1991), pp. 198–205.
[23] T.J.R. Hughes, A.N. Brooks. *A multidimensional upwind scheme with no crosswind diffusion*. in: Finite Element Methods for Convection Dominated Flows (Hughes, T.J.R., ed.), New York, ASME, 1979.
[24] C. Johnson, U. Nävert, J. Pitkäranta. *Finite element methods for linear hyperbolic problems*. Comput. Methods Appl. Mech. Engrg., 45 (1984), pp. 285–312.
[25] C. Johnson. Numerical Solution of Partial Differential Equations by the Finite Element Method, Combridge Univ. Press, Cambridge, 1987.
[26] A. Majda, P. Souganidis. *Flame fronts in a turbulent combustion model with fractal velocity fields*. Comm. Pure Appl. Math., 51 (1998), pp. 1337–1348.
[27] D. Mao, L. Shen, A. Zhou. *Adaptive finite element algorithms for eigenvalue problems based on local averaging type a posteriori error estimates*. Adv. Comput. Math., 25 (2006), pp. 135–160.
[28] U. Nävert. *A finite element method for convection-diffsion problems,* PhD thesis, Chalmers University of Technology Göteberg, 1982.
[29] J. Nolen, J. Xin. *Computing reactive front speeds in random flows by variational principle*. Physica D, 237 (2008), pp. 3172–3177.
[30] A. Novikov, L. Ryzhik. *Boundary layers and KPP fronts in a cellular flow*. Arch. Ration. Mech. Anal., 184 (2007), pp. 23–48.
[31] N. Peters, Turbulent Combustion, Cambridge University Press, Cambridge, 2000.
[32] M. Proctor, A. Gilbert, eds, "Lectures on Solar and Planetary Dynamos", Publications of the Newton Institute, Cambridge Univ Press, 1994.
[33] P. Ronney. *Some open issues in premixed turbulent combustion*. in: Modeling in Combustion Science (J. D. Buckmaster and T. Takeno, Eds.), Lecture Notes in Physics, Vol. 449, Springer-Verlag, Berlin, pp. 3–22, 1995.
[34] H-G Roos, M. Stynes, L. Tobiska. Robust Numerical Methods for Singularly Perturbed Differential Equations, Springer series in computational mathematics, 24, second edition, 2008.
[35] L. Ryzhik, A. Zlatos. *KPP pulsating front speed-up by flows*. Comm. Math. Sci., 5 (2007), pp. 575–593.
[36] L. Shen, J. Xin, A. Zhou. *Finite element computation of KPP front speeds in random shear flows in cylinders*. Multiscale Model. Simul., 7 (2008), pp. 1029–1041.
[37] L. Shen, J. Xin, A. Zhou. *Finite element computation of KPP front speeds in cellular and cat's eye flows*. J. Sci. Comput., 55(2), 2013, pp. 455-470.
[38] L. Shen, A. Zhou. *A defect correction scheme for finite element eigenvalues with applications to quantum chemistry*. SIAM J. Sci. Comput., 28 (2006), pp. 321–338
[39] G. Sivashinsky. *Cascade-renormalization theory of turbulent flame speed*. Combust. Sci. Tech., 62 (1988), pp. 77–96.
[40] R. Verfüth. A Review of a Posteriori Error Estimates and Adaptive Mesh-Refinement Techniques, Wiley-Teubner, New York, 1996.
[41] R. Verfüth. *Robust a posteriori error estimates for stationary convection-diffusion equations*. SIAM J. Numer. Anal., 43 (2005), pp. 1766–1782.
[42] F. Williams, *Turbulent combustion*. in: The Mathematics of Combustion (J. Buckmaster, ed.), SIAM, Philadelphia, pp. 97–131, 1985.
[43] J. Xin. An Introduction to Fronts in Random Media, Surveys and Tutorials in the Applied Mathematical Sciences, Vol. 5, Springer, 2009.
[44] J. Xin, Y. Yu. *Analysis and comparison of large time front speeds in turbulent combustion models*. http://arxiv.org/submit/255369, 2011.
[45] V. Yakhot. *Propagation velocity of premixed turbulent flames*. Comb. Sci. Tech., 60 (1988), pp. 191–214.
[46] A. Zlatos. *Sharp asymptotics for KPP pulsating front speed-up and diffusion enhancement by flows*. Arch Rat. Mech. Anal, 195 (2010), pp.441–453.
[47] A. Zlatos. *Reaction-diffusion front speed enhancement by flows*. Ann. Inst. H. Poincaré, Anal. Non Linaire, 28 (2011), pp. 711–726.

https://doi.org/10.1051/mmnp/20138311 Published online by Cambridge University Press

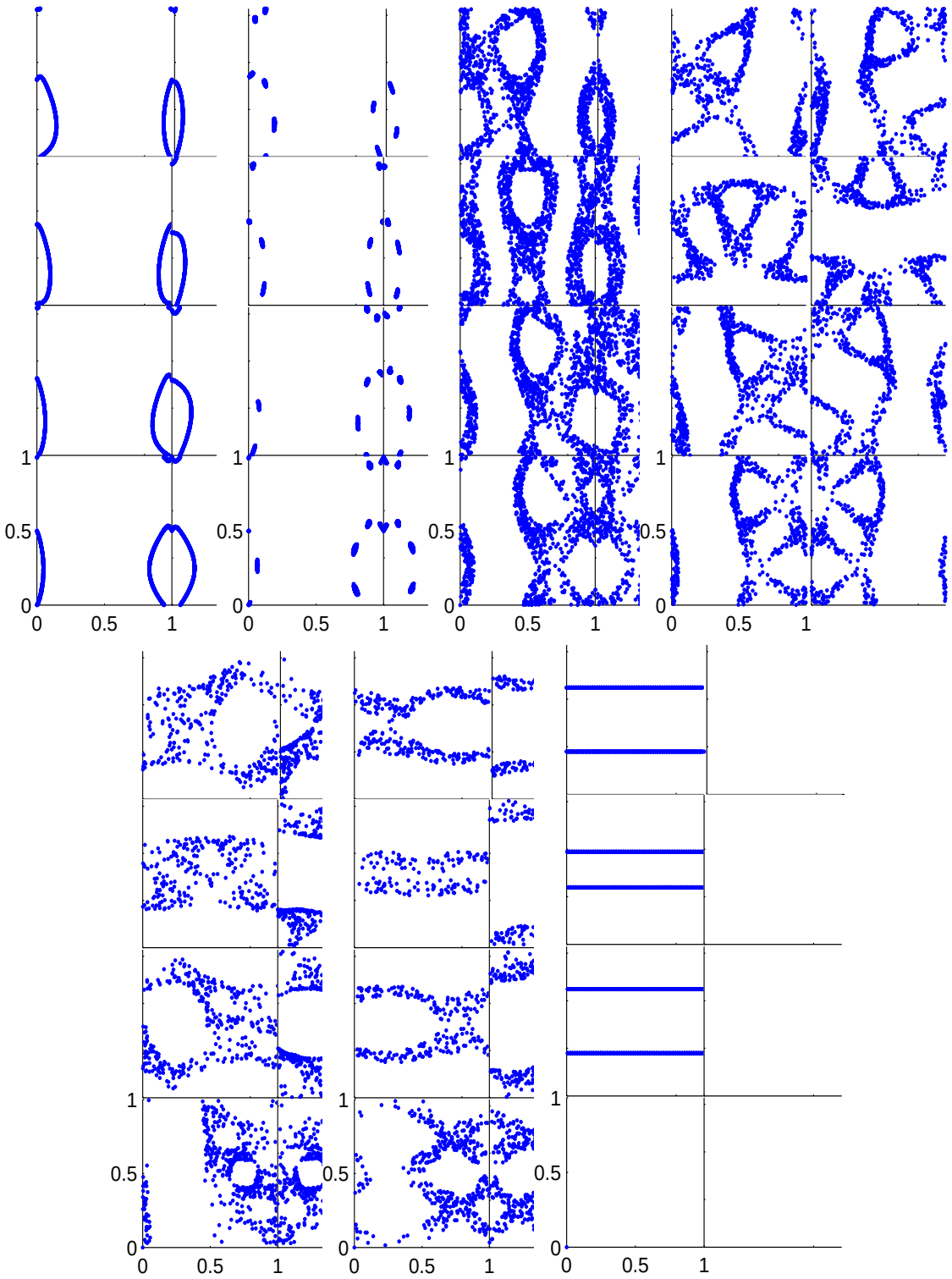


FIGURE 5. The Poincaré sections of the ABC flow. From left to right: $b = 4\sqrt{\frac{1}{3}}$, $3\sqrt{\frac{1}{3}}$, $2\sqrt{\frac{1}{3}}$, $\sqrt{\frac{1}{3}}$, $\frac{4}{8}\sqrt{\frac{1}{3}}$, $\frac{1}{8}\sqrt{\frac{1}{3}}$, 0.

https://doi.org/10.1051/mmnp/20138311 Published online by Cambridge University Press

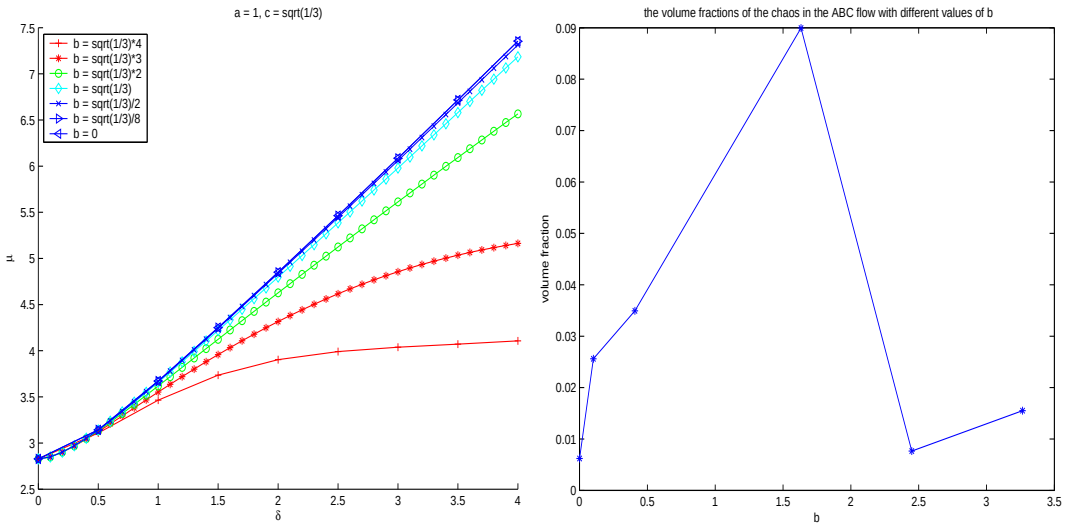


FIGURE 6. The left plot shows the front speed of ABC flow vs. δ at $a = 1.0$, $c = \sqrt{1/3}$ and different values of b in Figure 5. The right plot shows the volume fraction of chaotic streamlines vs. b.

https://doi.org/10.1051/mmnp/20138311 Published online by Cambridge University Press

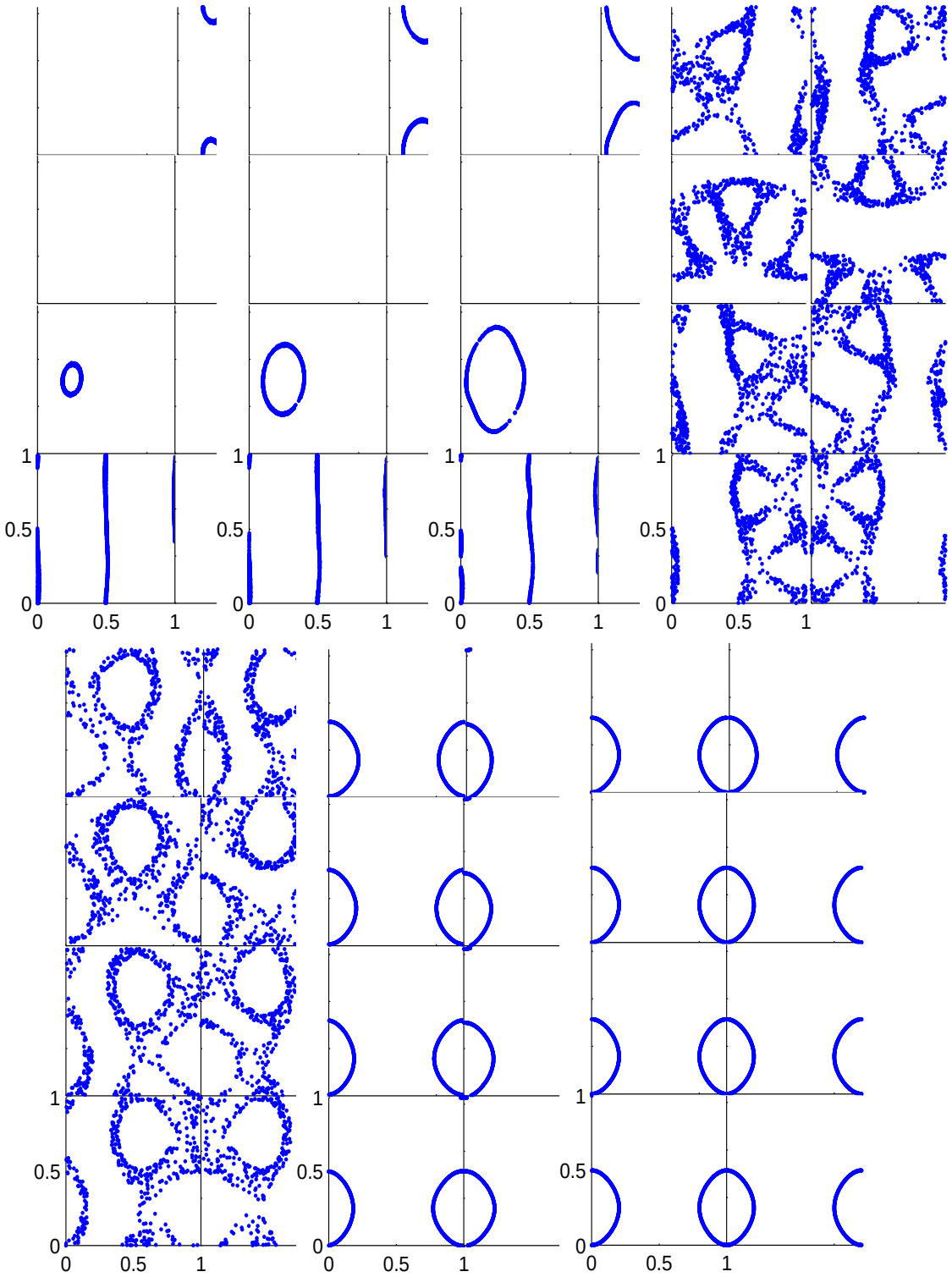


FIGURE 7. The Poincaré sections of ABC flow. From left to right: $a = 4, 3, 2, 1, \frac{4}{8}, \frac{1}{8}, 0$.

https://doi.org/10.1051/mmnp/20138311 Published online by Cambridge University Press

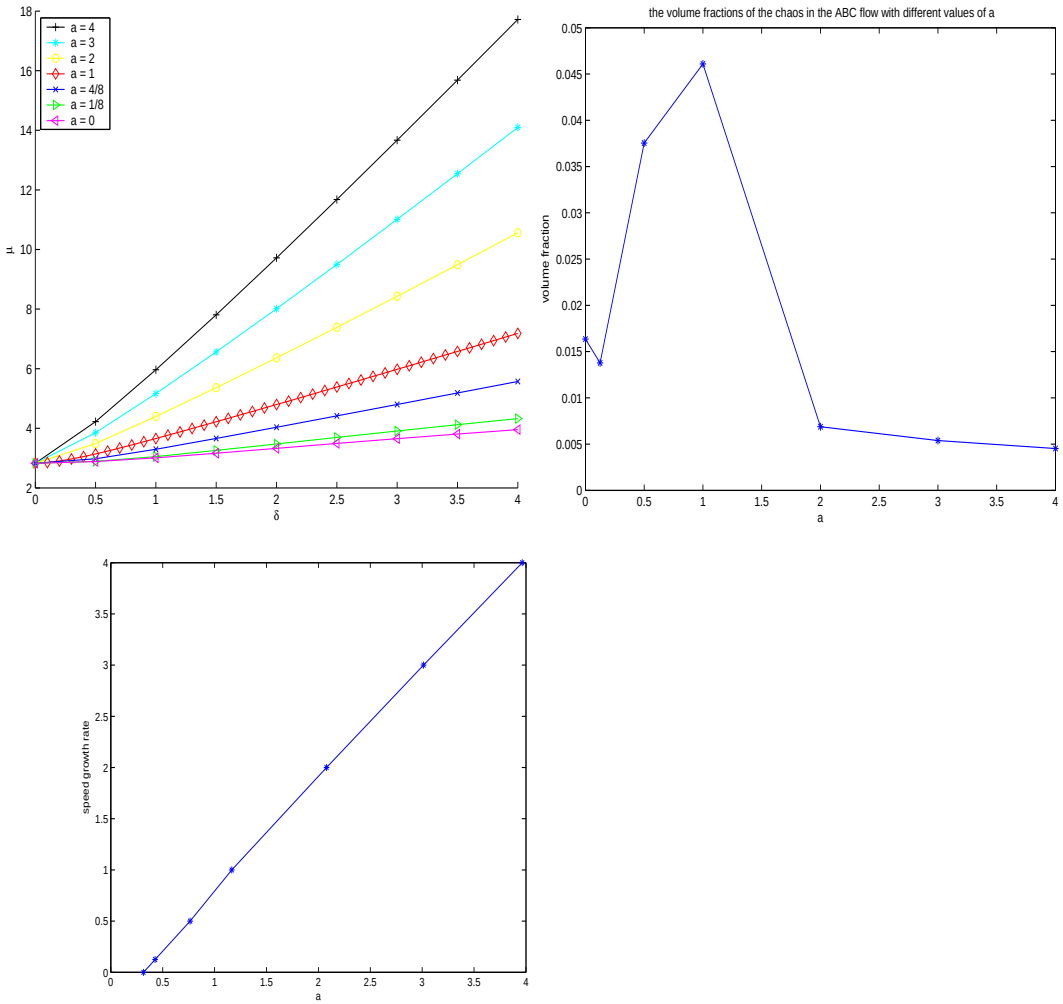


FIGURE 8. The upper left plot shows the front speed in ABC flow at $b = \sqrt{2/3}$, $c = \sqrt{1/3}$ and different values of a in Figure 7. The upper right plot is on the volume fraction of the chaotic streamlines at different values of a in Figure 7. The lower left panel is on the growth rate of the front speed as a is varied.

https://doi.org/10.1051/mmnp/20138311 Published online by Cambridge University Press